# Loss-of-function mutations in the IL-21 receptor gene cause a primary immunodeficiency syndrome

Daniel Kotlarz,[1,6] Natalia Ziętara,[1,6] Gulbu Uzel,[7] Thomas Weidemann,[12] Christian J. Braun,[1,6] Jana Diestelhorst,[1,6] Peter M. Krawitz,[13,14,15] Peter N. Robinson,[13,14,15] Jochen Hecht,[13,14,15] Jacek Puchałka,[6] E. Michael Gertz,[10] Alejandro A. Schäffer,[10] Monica G. Lawrence,[8] Lela Kardava,[9] Dietmar Pfeifer,[16] Ulrich Baumann,[2] Eva-Doreen Pfister,[2] Eric P. Hanson,[11] Axel Schambach,[3] Roland Jacobs,[4] Hans Kreipe,[5] Susan Moir,[9] Joshua D. Milner,[8] Petra Schwille,[12] Stefan Mundlos,[13,14,15] and Christoph Klein[1,6]

[1]Department of Pediatric Hematology/Oncology, [2]Department of Pediatric Kidney, Liver and Metabolic Diseases, [3]Department of Experimental Hematology, [4]Department of Clinical Immunology and Rheumatology, [5]Department of Pathology, Hannover Medical School, 30625 Hannover, Germany
[6]Department of Pediatrics, Dr. von Hauner Children's Hospital, Ludwig-Maximilians-Universität Munich, 80539 Munich, Germany
[7]Immunopathogenesis Section, Laboratory of Clinical Infectious Diseases, [8]Laboratory of Allergic Diseases, [9]Laboratory of Immunoregulation, National Institute of Allergy and Infectious Diseases; [10]National Center for Biotechnology Information; [11]National Institute of Arthritis and Musculoskeletal and Skin Diseases, National Insitutes of Health, Bethesda, MD 20892
[12]Biophysics Research Group, Technische Universität Dresden, 01062 Dresden, Germany
[13]Max Planck Institute for Molecular Genetics, 14195 Berlin, Germany
[14]Institute for Medical Genetics and Human Genetics, [15]Berlin-Brandenburg Center for Regenerative Therapies (BCRT), Charité Universitätsmedizin Berlin, 10117 Berlin, Germany
[16]Department of Hematology/Oncology, Genomics Core Laboratory, University Medical Center Freiburg, 79095 Freiburg, Germany

**Primary immunodeficiencies (PIDs) represent exquisite models for studying mechanisms of human host defense. In this study, we report on two unrelated kindreds, with two patients each, who had cryptosporidial infections associated with chronic cholangitis and liver disease. Using exome and candidate gene sequencing, we identified two distinct homozygous loss-of-function mutations in the interleukin-21 receptor gene (*IL21R*; c.G602T, p.Arg201Leu and c.240_245delCTGCCA, p.C81_H82del). The IL-21R$^{Arg201Leu}$ mutation causes aberrant trafficking of the IL-21R to the plasma membrane, abrogates IL-21 ligand binding, and leads to defective phosphorylation of signal transducer and activator of transcription 1 (STAT1), STAT3, and STAT5. We observed impaired IL-21–induced proliferation and immunoglobulin class-switching in B cells, cytokine production in T cells, and NK cell cytotoxicity. Our study indicates that human IL-21R deficiency causes an immunodeficiency and highlights the need for early diagnosis and allogeneic hematopoietic stem cell transplantation in affected children.**

CORRESPONDENCE
Christoph Klein:
christoph.klein@med.uni-muenchen.de

Abbreviations used: APD, avalanche photodiodes; DTT, diphtheria toxoid; EBV-BCL, EBV-transformed B cell lines; $\gamma_c$, common γ-chain; HSCT, hematopoietic stem cell transplantation; IVIG, intravenous immunoglobulin replacement; NGES, next-generation exome sequencing; PID, primary immunodeficiency; rh, recombinant human; STAT, signal transducer and activator of transcription; TT, tetanus toxoid.

Primary immunodeficiencies (PIDs) comprise a heterogeneous group of diseases characterized by global or selective susceptibility to infectious microorganisms (Casanova and Abel, 2007). Next-generation exome sequencing (NGES) technologies have provided a powerful tool to determine the molecular causes of rare Mendelian disorders (Ku et al., 2011). In the era of individualized medicine, the genetic etiology of rare disorders may be elucidated, providing a rational basis for tailored therapy.

IL-21R was originally identified by in silico homology screening (Ozaki et al., 2000). IL-21R

D. Kotlarz and N. Ziętara contributed equally to this paper.



The Rockefeller University Press $30.00
J. Exp. Med. 2013 Vol. 210 No. 3 433-443
www.jem.org/cgi/doi/10.1084/jem.20111229



The Journal of Experimental Medicine

binds to the common γ chain (*IL2RG*, $\gamma_c$) to transmit signals via JAK–signal transducer and activator of transcription (STAT) pathways (Spolski and Leonard, 2008). Immunophenotypic analysis of IL-21R–deficient mice revealed normal numbers of B, T, and NK cells (Kasaian et al., 2002; Ozaki et al., 2002; Fröhlich et al., 2009). However, IL-21 has been shown to regulate proliferation of lymphocytes (Parrish-Novak et al., 2002), B cell differentiation (Ettinger et al., 2005; Ozaki et al., 2002; Recher et al., 2011), cytotoxicity of NK cells (Kasaian et al., 2002), and differentiation of Th17 cells (Zhou et al., 2007). To date, no monogenic defects in IL-21 or IL-21R have been reported.

In this study, we identify loss-of-function mutations in *IL21R* in two kindreds, with two affected siblings each, who had cryptosporidiosis associated with chronic cholangitis and liver disease. Early diagnosis of IL-21R deficiency and allogeneic hematopoietic stem cell transplantation (HSCT) may prevent fatal complications.

## RESULTS AND DISCUSSION

### Clinical and immunological phenotype of family A

Patient 1 (P1; A.II-6) was referred as a 4-yr-old boy born to consanguineous parents of Lebanese descent (Fig. 1 A). He had chronic upper respiratory infections and developed end-stage liver disease. Due to progressive chronic cholangitis and biliary fibrosis, P1 underwent liver transplantation. Pathological analysis of his explanted liver showed complete hepatic cirrhosis (Fig. S1 A) and purulent cholangitis associated with marked epithelial and lymphoid hyperplasia (Fig. S1 B). Immunostaining was positive for cryptosporidia (Fig. S1 C).

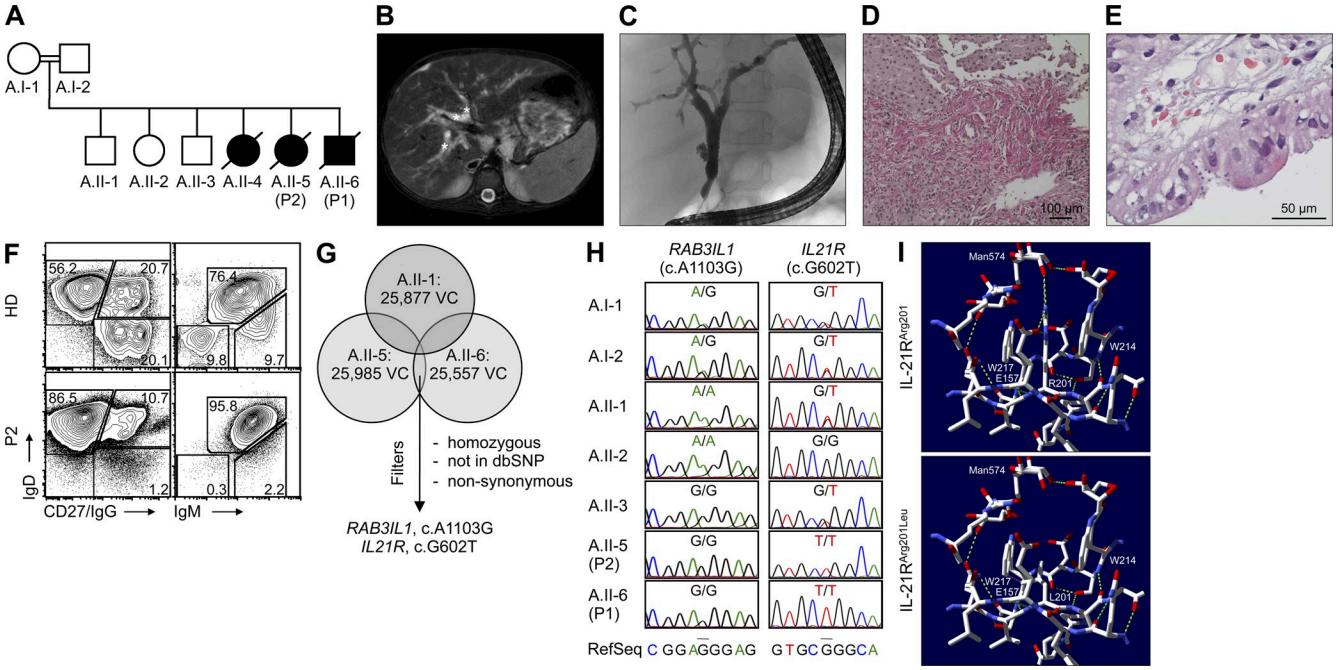


**Figure 1. Clinical and immunological phenotype, identification of IL-21R deficiency, and protein structure analysis in family A.** (A) Pedigree of family A. All affected children died secondary to infections and/or therapy-associated complications before the identification of the molecular genetic defect. (B) Abdominal magnetic resonance image revealing hepatomegaly and dilatation of intra- and extrahepatic bile ducts (*) in P2. (C) Endoscopic retrograde cholangiopancreatography demonstrated marked dilatation and irregularities of bile ducts in P2. (D) Histopathological analysis of liver biopsy from P2 showed that fibrous expansion of portal tracts with formation of septa accompanied by prominent ductular proliferation in the portal/lobular interphase was evident. (E) Duodenal biopsy from P2 showed numerous microorganisms ∼2 µm in size and confined to the luminal surface of enterocytes, consistent with cryptosporidiosis. (F) FACS analysis shows accumulation of $CD19^+IgD^{high}CD27^-IgG^-$ or $IgD^{high}IgM^{high}$ naive B cells in PBMCs isolated from P2 in comparison to a healthy donor. Plots are representative of 3 independent experiments. (G) Scheme of filtering approach for variant calls (VC, single-nucleotide variants and indels [insertion and deletions] <20 bp) from high-throughput sequencing of family members A.II-1, A.II-5, and A.II-6. All variants were filtered according to an autosomal recessive model of inheritance in a consanguineous family. Restricting the candidate set to rare, homozygous, nonsynonymous (NS), or splice site–affecting (SS) variants in the 38 MB CCDS exome resulted in identification of two potentially disease-causing variants: *RAB3IL1* and *IL21R*. (H) DNA Sanger sequencing of the *RAB3IL1* and *IL21R* genes confirmed segregation of the $IL\text{-}21R^{Arg201Leu}$ mutation with the disease phenotype in family A. (I) Structural analysis of wild-type (Arg201, R201; top) and mutant (Arg201Leu, L201; bottom) IL-21R based on the recently published Protein Data Bank structure 3TGX, illustrating IL-21 complexed with the extracellular domain of the IL-21R (Hamming et al., 2012). Hamming et al. number the amino acids in IL-21R with respect to the first amino acid in chain A of the structure 3TGX, while we number the amino acids in IL-21R in respect to the start of translation. Accordingly, the mutated Arg201 in P1 and P2 refers to Arg182 in (3TGX, Hamming et al., 2012). (top) The neighborhood of wild-type Arg201 displaying putative hydrogen bonds with a sugar chain and the Glu157 reside (green dashed lines). (bottom) The same region in the mutated IL-21R structure, illustrating that the Arg201Leu substitution is predicted to break these putative hydrogen bonds. Steric clashes are shown in purple.

Before liver transplantation, immunophenotyping of PBMCs revealed elevated numbers of B cells (2,444 $CD19^+$ cells/µl). Serum immunoglobulin levels were normal with the exception of elevated IgM (3.17 g/liter, normal range: 0.38–1.5) and IgE (1360 IU/ml, normal range: 2–60) levels. His post-transplant clinical course was complicated by abdominal abscesses, pneumonia, recurrent septicemia, systemic cytomegalovirus infection, and subsequent multiorgan failure leading to death on day +542.

P2, the 10-yr-old sister of P1 (A.II-5), showed similar symptoms and was referred for immunological workup. She had a history of recurrent pneumonia, chronic diarrhea, and failure to thrive. Clinical investigations revealed sinusitis (Fig. S1 D), *Helicobacter pylori*–associated gastritis (Fig. S1 E), and esophageal candidiasis (Fig. S1 F). Magnetic resonance imaging showed a markedly increased liver size, dilated biliary tract system, and lymphadenopathy (Fig. 1 B). Retrograde cholangiography studies confirmed a massive dilatation of the bile duct system (Fig. 1 C). The liver biopsy revealed extensive fibrosis (Fig. 1 D), as well as cryptosporidia in the bile ducts and duodenum (Fig. 1 E). Immunophenotyping of PBMCs revealed normal numbers of T, B, and NK cells (unpublished data). However, the population of immunoglobulin class-switched $IgG^+CD27^+$ B cells was reduced (Fig. 1 F), and the proportion of $CD3^+CD4^-CD8^-$ T cells (16%) was elevated (not depicted). The patient had slightly below-normal serum IgG levels (4.95 g/liter; normal range, 5.2–12.9 g/liter) and above-normal IgE levels (2,010 IU/ml; normal range, 6–120 IU/ml). P2 underwent HLA-identical HSCT, and her post-transplant course was complicated by increased cholangitis, cytomegalovirus infection, and graft rejection. A second transplant was performed, but the patient died on day +84 secondary to multiorgan failure.

The predominant clinical findings in both siblings of family A were severe cholangitis and liver fibrosis associated with cryptosporidial infection. Chronic cryptosporidia-associated cholangitis can be seen in T cell deficiency, in particular in patients with HIV infection (Wolska-Kusnierz et al., 2007), HLA class II deficiency (Klein et al., 1993), and hyper-IgM syndrome (Wolska-Kusnierz et al., 2007). These differential diagnoses were excluded by standard immune assays (HIV, HLA class II deficiency) and Sanger sequencing (*CD40*, *CD40LG*).

### Genetic analysis and protein structure studies in family A

Exomes from individuals A.II-1, A.II-5, and A.II-6 in kindred A were enriched and subjected to NGES. Among all detected rare, nonsynonymous sequence variants, two were homozygous in both patients, but not in one unaffected sibling, which is consistent with recessive inheritance: IL-21R$^{Arg201Leu}$ and RAB3IL1$^{Lys368Arg}$ (Fig. 1 G and Table S1). In parallel, we conducted SNP-based homozygosity mapping, analyzing genomic DNA from all healthy siblings and both patients (A.II-5, A.II-6), yielding four perfectly segregating regions more than 1 Mbp in size on chromosomes 5, 12 (two intervals), and 16 (largest interval).

In contrast to the IL-21R$^{Arg201Leu}$ mutation (chromosome 16), the variant in *RAB3IL1* (*RAB3A interacting protein [rabin3]-like 1*, chromosome 11) is not located in a homozygous interval and does not segregate with the disease phenotype, as confirmed by Sanger sequencing (Fig. 1 H). In silico analysis using SIFT (Ng and Henikoff, 2002) and PolyPhen (Ramensky et al., 2002) predicted that the IL-21R$^{Arg201Leu}$ mutation is deleterious in respect to function, whereas the *RAB3IL1* sequence variation is benign according to both algorithms. Thus, *IL21R* was considered as the causative gene.

The crystal structure of the extracellular domain of the human IL-21R complexed to IL-21 has recently been elucidated (Hamming et al., 2012). When IL-21 binds to IL-21R, the residue Arg201 is sandwiched between Trp214 and Trp217 (Hamming et al., 2012), two tryptophans in the TrpSerXaaTrpSer (WSXWS) motif that are characteristic of class I cytokine receptors (Hilton et al., 1996). Fig. 1 I (top) depicts the neighborhood of Arg201 in the predicted structure of IL-21R, showing putative hydrogen bonds between Arg201 and a sugar chain attached to Asn73, as well as a hydrogen bond between Arg201 and Glu157. In comparison, the substitution of an uncharged Leu is predicted to break these bonds (Fig. 1 I, bottom). The protein structure validation tool MolProbity in conjunction with Probe reports several severe steric clashes between Leu201 and Trp217, the worst of which is a clash of 1.6 Å. In contrast, only a single clash of 0.42 Å is reported between Arg201 and Trp217, suggesting that the Arg201Leu substitution is destabilizing. Moreover, PoPMuSiC uses a different method to predict that the Arg201Leu substitution leads to a destabilizing $\Delta\Delta G$ of 0.36 kcal/mol.

Because the WSXWS motif has been implicated in proper protein folding and exiting of the endoplasmic reticulum (Hilton et al., 1996), we assumed that the IL-21R$^{Arg201Leu}$ mutation might result in defective cell membrane trafficking. To test this hypothesis, we studied HeLa cells coexpressing the $\gamma_c$ along with a C-terminal wild-type or mutant (Arg201Leu) IL-21R-eGFP fusion protein using high-resolution confocal microscopy (Fig. 2, A and B). Wild-type IL-21R-eGFP showed plasma membrane expression and accumulations in perinuclear membrane systems; a characteristic feature also observed for other GFP-tagged cytokine receptors such as IL-4RA, IL-13RA1, and $\gamma_c$ (Weidemann et al., 2011). In contrast, the subcellular distribution of the mutated IL-21R-eGFP appeared more homogeneous. High-resolution avalanche photodiodes (APD) imaging confirmed trafficking into the endoplasmic reticulum (ER) and the nuclear membrane, indicating misfolding, impaired processing, or misguided trafficking in the secretory pathway (Fig. 2 A). Furthermore, when cells were engineered to express an RFP-tagged JAK3 construct to visualize interaction with $\gamma_c$ at the plasma membrane, colocalization of JAK3 and IL-21R-eGFP could be documented in cells expressing wild-type IL-21R-eGFP, but not in cells expressing the mutant fusion protein (Fig. 2 B). To further assess the consequences for ligand recognition,

we used a fluorescently labeled recombinant human (rh) IL-21 protein (IL-21-Atto647N) and measured surface binding by FACS (Fig. 2 C, top). Only cells expressing $\gamma_c$ and wild-type IL-21R-eGFP, but not cells expressing $\gamma_c$ alone or cells expressing $\gamma_c$ and mutant IL-21R-eGFP, were able to bind the cognate ligand IL-21-Atto647N. The ligand-binding signal for the wild-type receptor clearly correlated with eGFP expression. A similar correlation was seen in respect to eGFP and IL-21R surface expression in wild-type IL-21R-eGFP–transduced HeLa cells, but not in cells transduced with mutant IL-21R-eGFP (Fig. 2 C, bottom). These experiments suggest that the mutant IL-21R$^{Arg201Leu}$ is misfolded, retained in the endoplasmic reticulum, and does not properly traffic to the plasma membrane.

N-linked glycosylation of IL-21R appears to be a prerequisite for its proper cell surface expression (Hamming et al., 2012). Western blot studies of protein extracts derived from EBV-transformed B cell lines (EBV-BCL) of P2 revealed a different molecular weight pattern of the IL-21R in comparison to healthy donors (Fig. 2 D). Similar results were observed in HeLa cells that were lentivirally engineered to overexpress $\gamma_c$ along with IL-21R$^{Arg201}$ or IL-21R$^{Arg201Leu}$ (unpublished data). Treatment of the protein extracts from EBV-BCL with PNGaseF and EndoH before electrophoretic separation resulted

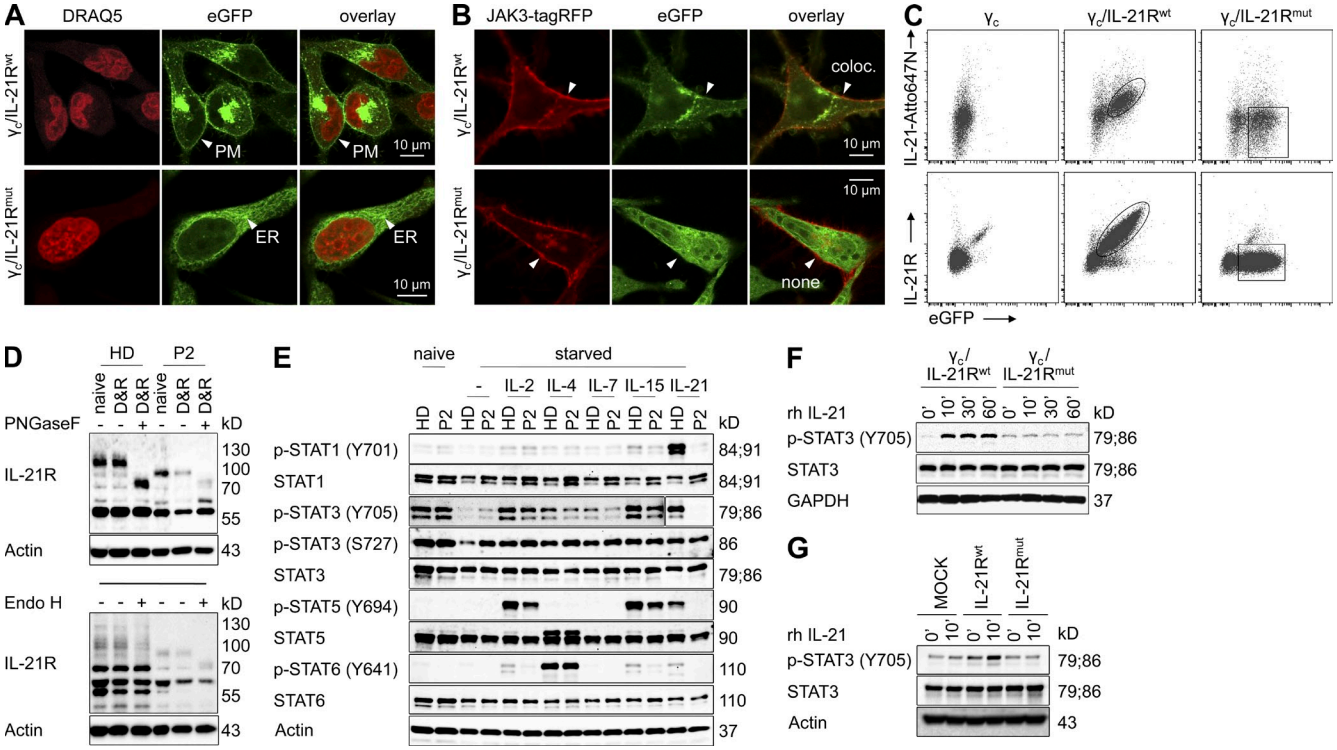


**Figure 2. Defective IL-21R subcellular distribution, N-linked glycosylation, and signal transduction in family A.** (A) High-resolution APD imaging in HeLa cells expressing wild-type (wt, Arg201) or mutant (mut, Arg201Leu) C-terminal, eGFP-fused, IL-21R demonstrated distinct subcellular distribution. In contrast to the IL-21R$^{wt}$-eGFP, which was expressed at the plasma membrane (PM; arrowheads), the IL-21R$^{mut}$-eGFP protein was dispersed in the endoplasmic reticulum (ER; arrow heads) and did not traffic to the plasma membrane. Nuclei were stained using DRAQ5. (B) High-resolution APD imaging in HeLa cells expressing wild-type (wt, Arg201) or mutant (mut, Arg201Leu) IL-21R-eGFP illustrates incomplete colocalization of IL-21R$^{Arg201Leu}$ with transiently expressed RFP-tagged JAK3. (C) FACS analysis gated on intact HeLa cells that were lentivirally engineered to overexpress either $\gamma_c$/IL-21R$^{wt}$-eGFP (Arg201) or $\gamma_c$/IL-21R$^{mut}$-eGFP (Arg201Leu). The top image reveals that IL-21-Atto647N ligand binding correlates with the magnitude of eGFP expression in HeLa cells expressing $\gamma_c$/IL-21R$^{wt}$-eGFP (Arg201), but not in $\gamma_c$/IL-21R$^{mut}$-eGFP (Arg201Leu)–transduced HeLa cells. The bottom image demonstrates that IL-21R surface staining correlates with the eGFP expression in $\gamma_c$/IL-21R$^{wt}$-eGFP (Arg201)–transduced HeLa cells, whereas HeLa cells expressing $\gamma_c$/IL-21R$^{mut}$-eGFP (Arg201Leu) showed aberrant IL-21R surface expression. (D) Western blot analysis of IL-21R expression in EBV-BCL from P2 in comparison to healthy donors. Protein lysates were treated with PNGaseF (top; 60 min, 30 IU/µl) or Endo H (bottom; 60 min, 100 IU/µl) before electrophoresis. Data shown are representative of three independent experiments. D, denaturation buffer; R, reaction buffer. (E) Western blot analysis of STAT signaling in EBV-BCL from P2 and healthy donor (HD) upon stimulation with indicated $\gamma_c$-related cytokines: IL-2 (100 ng/ml), IL-4 (100 ng/ml), IL-7 (100 ng/ml), IL-15 (10 ng/ml), and IL-21 (10 ng/ml). Please note that for detection of STAT3 phosphorylation (Tyr705, Y705) upon stimulation with IL-2, IL-4, IL-7, and IL-15, a longer exposure was used compared with stimulation with IL-21. Data are representative of two independent experiments, and defective STAT phosphorylation in P2 upon stimulation with IL-21 was confirmed in three additional experiments. (F) Western blot analysis of STAT3 phosphorylation (Tyr705, Y705) in IL-21–stimulated HeLa cells that were lentivirally transduced with $\gamma_c$ along with either IL-21Rwt or IL-21Rmut. Data are representative of three independent experiments. (G) Lentiviral gene transfer of wild-type IL-21R in patient's fibroblasts induces IL-21–mediated STAT3 signaling. Western blot analysis of STAT3 phosphorylation (Tyr705, Y705) in IL-21–stimulated dermal fibroblasts that were lentivirally transduced with wild-type or mutated IL-21R (Arg201Leu). Data depicted are representative of four independent experiments. GAPDH or actin were used as loading controls in D–G.

in removal of N-linked oligosaccharides, indicating that this expression pattern of IL-21R is associated with differences in N-glycosylation (68–130 kD; Fig. 2 D).

### Defective IL-21R–mediated signaling in family A

We stimulated EBV-BCL from P2 with rh IL-21 and determined phosphorylation levels of STAT1 (Tyr701), STAT3 (Tyr705), and STAT5 (Tyr694). Phosphorylation of all three downstream mediators was severely abrogated in the patient (Fig. 2 E). Further, STAT phosphorylation via other $\gamma_c$-related cytokines (IL-2, IL-4, and IL-15) was not affected by the IL-21R mutation in EBV-BCLs.

To confirm that the IL-21R$^{Arg201Leu}$ mutation is responsible for defective STAT signaling, we analyzed STAT3 phosphorylation (Tyr705) upon stimulation with rh IL-21 in HeLa cells expressing either the wild-type (IL-21Rwt-$\gamma_c$) or the mutant (IL-21Rmut-$\gamma_c$) heterodimeric IL-21R by Western blot analysis (Fig. 2 F). The IL-21Rwt-$\gamma_c$ heterodimer induced phosphorylation of STAT3 in HeLa cells, whereas no phosphorylation was seen in cells expressing the mutant IL-21R, indicating that the Arg201Leu mutation abrogates IL-21R–mediated signal transduction. In addition, lentiviral transduction of wild-type IL-21R, but not of mutated IL-21R, induced STAT3 phosphorylation upon exposure to rh IL-21 in primary fibroblasts of P2 (Fig. 2 G).

### Functional consequences of human IL-21R deficiency on B, NK, and T cells in P2 from family A

In light of decreased numbers of class-switched B cells ($IgG^+CD27^+$) in P2, we analyzed the functional consequences of IL-21R deficiency in naive B cells ($CD19^+IgD^{high}IgG^-CD27^-$) in vitro. In comparison to healthy donors, the patient's B cells had a markedly reduced proliferative capacity (Fig. 3 A). Furthermore, no induced surface expression of IgG and IgA could be detected in IL-21R–deficient B cells, whereas naive B cells from healthy donors underwent IL-21–mediated

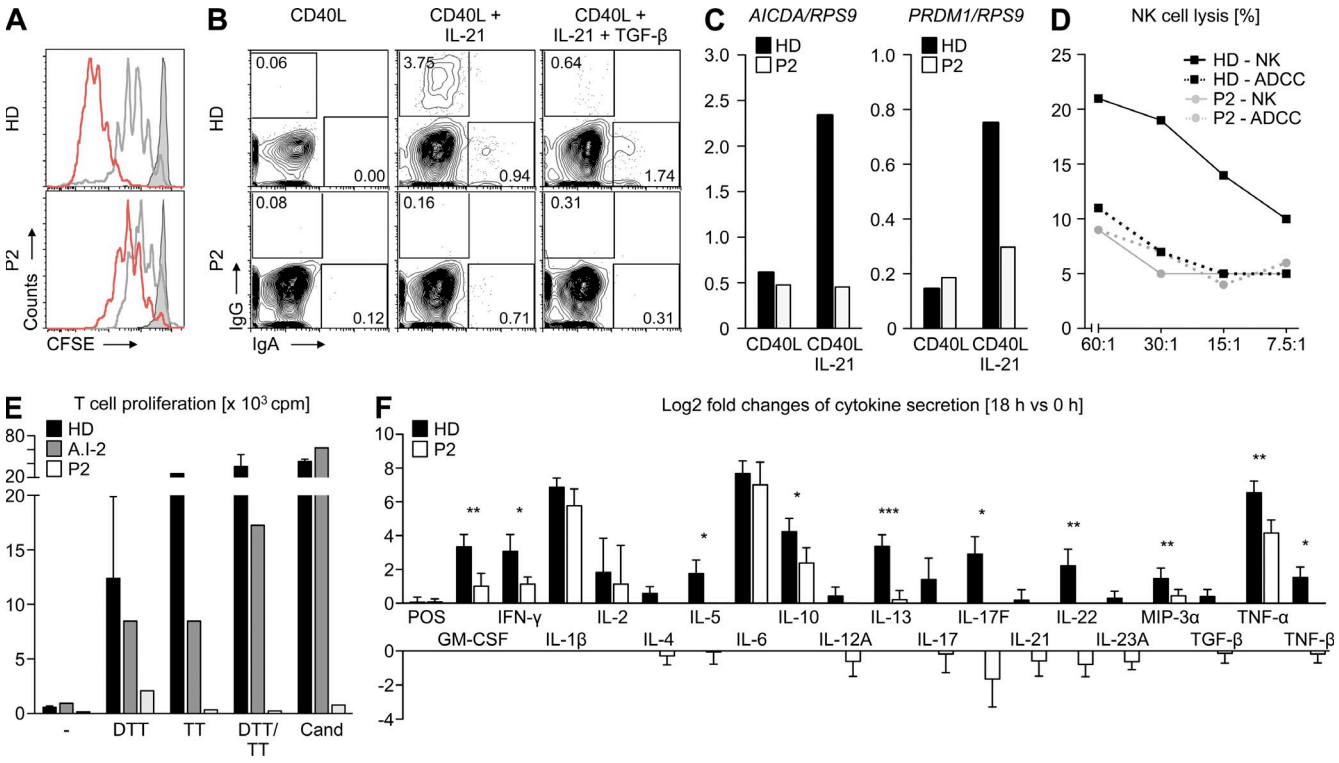


**Figure 3. Functional consequences of aberrant IL-21R signaling in B and T cells from P2 of family A.** (A) Representative FACS analysis showing proliferation of IL-21R–deficient naive B cells that were co-cultured with 3T3 CD40L-expressing cells and stimulated with anti-IgM beads (50 ng/ml), CpG (50 nM), and rh IL-2 (20 U/ml) in the presence or absence of rh IL-21 (30 ng/ml) for 6 d. Histograms illustrate proliferation of CFSE-labeled B cells isolated from healthy donors (HD) and patient (P2, A.II-5). Gray shaded, unstimulated B cells; gray line, CD40L-stimulated B cells; red line, CD40L-/IL-21–stimulated B cells. (B) FACS analysis of immunoglobulin class-switch in naive IL-21R–deficient B cells upon stimulation with rh IL-21 for 6 d. (C) Expression of *AICDA* and *PRDM1* mRNA was determined in CD40L-/IL-21–stimulated B cells after 6 d using Real-time PCR analysis. Values represent the expression of respective genes in relation to *RPS9* (ribosomal protein S9). (D) Analysis of NK cell cytotoxicity and antibody-dependent cellular cytotoxicity (ADCC) using $^{51}Cr$-release assay. (E) T cell proliferative response to stimulation with antigens was determined by [$^3H$]-thymidine incorporation assay. PBMCs isolated from healthy donors ($n = 4$), father, and P2 were stimulated with *C. albicans* (Cand), DTT, and TT. Depicted data represent average of duplicates and are representative of two independent experiments. (F) Secretion of multiple cytokines in IL-21R–deficient T cells measured by protein array. Data shown are compiled from two independent experiments. The bars render logarithms (to the base of 2) of fold changes between unstimulated cells and cells upon stimulation with anti-CD3/anti-CD28 for 18 h. For each bar, the 95% confidence interval is given. Asterisks indicate cytokines for which the 95% (*), 99% (**), and 99.9% (***) confidence intervals do not overlap.

immunoglobulin class-switch events (Fig. 3 B). In addition, upon stimulation with IL-21, the patient's B cells showed impaired mRNA up-regulation of *AICDA* and *PRDM1*, two genes associated with isotype class-switch and B cell differentiation (Fig. 3 C). In comparison to healthy individuals, IL-21R–deficient NK cells from P2 showed impaired NK cell lysis of $^{51}$Cr-labeled K562 target cells, but antibody-dependent cellular cytotoxicity was unaffected (Fig. 3 D). T cell proliferation upon stimulation with anti-CD3 and mitogens (PHA, ConA, and PWM) in P1 and P2 was comparable to healthy donors (unpublished data). However, T cell proliferation in response to antigens such as diphtheria toxoid (DTT), tetanus toxoid (TT), and *Candida albicans* was impaired in case of P2 (Fig. 3 E). Specific antibody responses to immunization antigens (DTT, TT, and *Haemophilus influenzae* type B) were reduced (unpublished data).

Because chronic cryptosporidiosis is seen in association with T cell deficiency, we performed transcriptome analysis on anti-CD3/anti-CD28–stimulated peripheral blood lymphocytes from P2. We identified changes in the expression level of cytokines after 6, 12, and 18 h of stimulation (in total 78 genes). In particular, we observed no increase in the expression levels of Th17-associated cytokines (e. g., IL-17 and IL-22) in IL-21R–deficient cells (Table S2).

To validate these findings on the protein level, we measured the secretion of effector cytokines in supernatants using a protein array. IL-21R–deficient T cells from P2 had a defect in respect to secretion of multiple cytokines, including the Th17-associated cytokines IL-17F and IL-22 (Fig. 3 F). These results are consistent with findings in murine IL-21–deficient T cells (Nurieva et al., 2007) and may explain, in part, increased susceptibility to cryptosporidial infections.

### IL-21R deficiency in an unrelated family B

P3 (B.II-1, a 13-yr-old boy) and P4 (B.II-2, an 8-yr-old boy) were born to consanguineous parents from Colombia (Fig. 4 A) and were included in this study based on the close resemblance of the clinical and immunological phenotype to kindred A.

P3 had recurrent otitis media and multiple episodes of pneumonia (e.g., *Pseudomonas aeruginosa* and *Pneumocystis jirovecii*) throughout childhood, leading to bronchiectasis

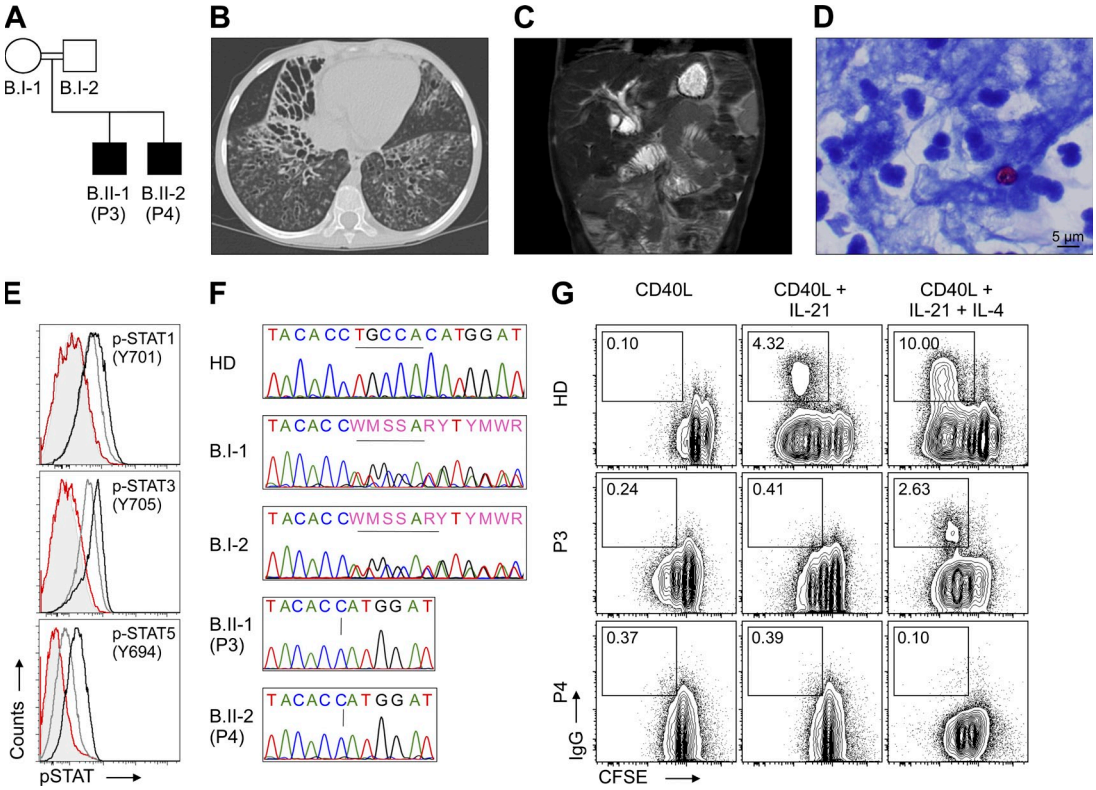


**Figure 4. Clinical and immunological phenotype and identification of IL-21R deficiency in family B.** (A) Pedigree of family B. (B) Chest computed tomography (CT) showing extensive bronchiectasis. *P. aeruginosa* was cultured from bronchoalveolar lavage after this CT. (C) Magnetic resonance imaging/magnetic resonance cholangiopancreatography of the liver showing extensive intra and extrahepatic biliary duct dilatation. (D) Modified acid fast staining of bronchoalveolar lavage showing abundant neutrophils and *Cryptosporidium*. (E) FACS analysis of STAT phosphorylation (p-STAT1 Y701, p-STAT3 Y705, and p-STAT5 Y694) in PBMCs isolated from healthy donors (HD), mother (B.I-1), and P3 upon stimulation with rh IL-21. Black line, HD, rh IL-21; dark gray line, B.I-1, rh IL-21; light gray shaded; P3, unstimulated; red line; P3, rh IL-21. (F) DNA Sanger sequencing revealed a homozygous deletion in the *IL21R* gene (c.240_245delCTGCCA, p.C81_H82del) in P3 and P4. In contrast, the parents showed a heterozygous genotype. (G) FACS analysis of B cell proliferation and class-switch in P3 and P4 upon stimulation with rh IL-21.

(Fig. 4 B). At age 10, he developed intrahepatic and extrahepatic biliary ductal dilation consistent with clinical symptoms of cholangitis (Fig. 4 C). Lymphocyte subsets and serum immunoglobulin levels were within normal range except elevated IgE (24425 IU/ml) and low IgG (764 mg/dl) levels. T cell proliferation in response to TT was reduced, whereas response to *C. albicans* was normal. Antibody responses to TT, DTT, and 23-valent pneumococcal vaccines were decreased. At age 11, intravenous immunoglobulin replacement (IVIG) was initiated because of low IgG levels (625 mg/dl). *Cryptosporidium* was detected in stool samples, sputum, and bronchoalveolar lavage (Fig. 4 D).

P4 had recurrent otitis media and multiple episodes of pneumonia starting at age 3. He developed diarrhea, malabsorption, and malnutrition by 3.5 yr of age. Liver disease manifested at age 4. *Cryptosporidium* was first detected in stool and subsequently seen in duodenal and esophageal biopsies, as well as in sputum at age 6. A liver biopsy showed preserved hepatic architecture, but sparse portal chronic inflammatory infiltrates and diffuse macrovesicular steatosis. He was started on IVIG at age 7, when his IgG level was 325 mg/dl. His IgE levels were slightly increased (166 IU/ml). Before IVIG, he had poor antibody response to pneumococcal vaccine, but normal response to TT vaccine. Lymphocyte subset counts were in normal ranges except for slightly decreased $CD8^+$ cells (153 $CD8^+$ T cells/μl). T cell proliferation in response to PHA and ConA was slightly diminished (PHA: 89444, reference > 138,000 cpm; ConA: 68287, reference > 99,500 cpm), but PWM was normal. T cell response to antigens (TT and *C. albicans*) and NK cell function was decreased. He had several episodes of bacteremia and systemic *C. albicans* infections, two episodes of *P. jirovecii* pneumonia, recurrent *P. aeruginosa* and *Streptococcus pneumoniae* infections of the lungs, persistent gastrointestinal norovirus infection, and a hematogenous dissemination of pulmonary *Mycobacterium massiliense* infection. Corticosteroid therapy, initiated empirically to control inflammation, may have aggravated the susceptibility to infection.

In kindred B, a flow cytometry screen for cytokine signaling abnormalities showed a loss of IL-21–mediated signaling. Similar to P2, no phosphorylation of STAT1 (Tyr701), STAT3 (Tyr705), and STAT5 (Tyr694) could be documented in patient PBMCs upon stimulation with rh IL-21 (Fig. 4 E). Candidate gene sequencing identified a homozygous deletion in exon 4 of the *IL21R* gene (c.240_245delCTGCCA; p.Cys81_His82del; Fig. 4 F). No mutations in the coding region of the *RAB3IL1* gene were detected in either patient by Sanger sequencing. Protein structure analysis by Hamming et al. (2012) shows that the amino acid Cys81, deleted in P3 and P4, is needed to form a disulfide bridge with Cys65, suggesting that this deletion results in misfolding of the mutated IL-21R protein.

Functional B cell assays showed that P3 and P4 had defective IL-21–dependent immunoglobulin class-switch (Fig. 4 G). These in vitro data correspond to decreased serum IgG levels and defective production of antigen-specific IgG in vivo. Impaired NK cell–mediated cytotoxicity has also been documented in P4, whereas P3 reportedly had normal NK cell function (unpublished data).

Collectively, the identified IL-21R–deficient patients presented with a rare PID characterized by B and T cell defects, and variable dysfunction of NK cells. Unlike $\gamma_c$-deficiency, IL-21R deficiency is not associated with severe defective T cell developmental defects or severe combined immunodeficiency. Nevertheless, IL-21R deficiency is a life-threatening disease. Clinically, all patients had recurrent respiratory and gastrointestinal infections. Chronic cholangitis and liver disease associated with chronic cryptosporidial infections were remarkable findings. Analysis of mouse models revealed that IL-21 is important for a durable, initial T cell response to viral infections (Fröhlich et al., 2009) and for memory B cells (Rankin et al., 2011). T and B cell dysfunction in IL-21R–deficient patients may explain the susceptibility to chronic infections. The clinical phenotype of liver fibrosis is unexpected because a murine study showed that *Il21r*$^{-/-}$ mice are less susceptible to liver fibrosis than wild-type mice (Pesce et al., 2006). The phenotypic difference in liver fibrosis could be caused by either inter-species differences or to the cryptosporidial infection observed in our patients. Further, we cannot completely rule out the possibility that interferences of the mutated IL-21R and other $\gamma_c$-related cytokine receptors might play a modulatory role on the clinical and/or immunological phenotype in our patients.

In view of the refractory course and a suspected immunodeficiency, an HLA-identical HSCT was performed in P2. However, her posttransplant course was complicated by secondary infections leading to death. P3 and P4 are alive, but too ill for allogeneic HSCT. Therefore, an early diagnosis and HSCT might be of critical importance for IL-21R–deficient patients to prevent multiorgan complications. Future studies are required to characterize the full clinical and immunological phenotype of this disorder, in particular in subjects not infected with cryptosporidia.

The discovery and characterization of the first patients with IL-21R deficiency highlight the critical role of IL-21–dependent signaling for the human immune system and expand the spectrum of $\gamma_c$-related immunodeficiencies. Our study also exemplifies the important role of NGES complemented by cell-based screening assays in the discovery of genetic defects causing novel, rare Mendelian diseases.

## MATERIALS AND METHODS

**Patients.** Peripheral blood samples of patients, their unaffected first-degree relatives, and healthy volunteers were obtained upon written (parental) consent. The study protocols were approved by the Institutional Review Board at Hannover Medical School, Germany, and the National Institute of Allergy and Infectious Diseases Intramural Institutional Review Board in Bethesda, MD.

**Homozygosity mapping.** DNA samples from two obligate carrier parents, two affected children (one already deceased at the time of genotyping), and three unaffected children from family A were genotyped using the Affymetrix Genome-Wide Human SNP 6.0 Mapping Array, and genotypes were called using the same protocols as for pedigree B in Glocker et al. (2009). Using the software findhomoz, we sought perfectly segregating regions defined

as those where the two affected children are homozygous for the same genotype and the five unaffected individuals have genotypes different from the affected individuals.

**Exome sequencing.** Genomic DNA of one unaffected sibling (A.II-1) and two affected siblings (A.II-5, A.II-6) from family A was enriched for the target region of all human CCDS (consensus coding sequence project) exons using Agilent's SureSelect Human All Exon kit (Agilent Technologies) according to the manufacturer's protocol, followed by single-read cluster generation on the Cluster Station (Illumina). The captured, purified, and clonally amplified library targeting the exome was then sequenced on an Illumina Genome Analyzer II. For each sample, two lanes of 100 bp single-read sequencing were performed following the manufacturer's protocol resulting in more than 5 Gb of high-quality, short-read sequence data per individual.

**Exome sequence analysis.** The raw short read sequence data were reduced to unique sequences and aligned to the human genome (hg19) using Novoalign. The percentage alignment of the reads to the targeted exome was calculated using Perl scripts and Bedtools (Quinlan and Hall, 2010). In each patient from family A, ∼90% of the target regions were covered by >10 unique sequence reads. SAMtools and Perl scripts were used for the detection of single nucleotide variants and small indels (insertions and deletions <20 bp) on the short-read BAM alignment files (Li et al., 2009; Krawitz et al., 2010). All detected variants were reduced to family-specific, rare variants by filtering out polymorphisms in dbSNP (build132), including those reported in HapMap or the first major release from the 1000 Genomes Project. Assuming a pattern of autosomal recessive inheritance with 100% penetrance of the phenotype, we filtered for genes with homozygous or compound heterozygous nonsynonymous variants in the affected siblings, but not in the unaffected sibling.

Possibly causative sequence variants were analyzed with PolyPhen 2 (Ramensky et al., 2002) and SIFT (Ng and Henikoff, 2002). We used default settings, except that when using SIFT, we identified the homologous sequences and aligned the sequences using PSI-BLAST (Altschul et al., 1997), instead of using the precomputed matching sequences and alignment. Any variants scoring <0.05 with SIFT were predicted as deleterious.

**DNA extraction, PCR and targeted DNA sequencing.** DNA of members of kindred A was isolated using the Peqlab Gold Tissue DNA kit (Peqlab) according to the manufacturer's instructions. DNA samples from family B were provided by NIAID/National Institutes of Health. For DNA Sanger sequencing, coding regions of the *IL21R* (ENST00000395755) and *RAB3IL1* (ENST00000394836) genes were amplified using specific forward and reverse primers (Table S3).

PCR conditions were as follows: initial denaturation at 95°C for 5 min, 35 cycles of 95°C for 30 s, 56°C for 30 s, and 72°C for 1 min, and final elongation at 72°C for 10 min. Amplicons were purified using the QIAquick PCR purification kit (QIAGEN) and sequenced with the ABI PRISM BigDye Terminator v3.1 Cycle Sequencing kit (Applied Biosystems). DNA sequencing was accomplished with an ABI 3130xl DNA Sequencer (Applied Biosystems). The sequence reads were analyzed with DNA Sequencing Analysis software version 3.4 (Applied Biosystems) and DNASTAR Lasergene (DNASTAR).

**Structural analysis on wild-type (Arg201) and mutated (Arg201Leu) IL-21R.** To analyze the mutant IL-21R$^{Arg201Leu}$ protein, we followed part of a plan originally suggested by (Thusberg and Vihinen 2006) for analyzing structural effects of amino acid substitutions, as refined in another more recent study of the structure changes caused by amino acid substitutions observed in patients with immunodeficiencies (Salzer et al., 2009). Because the residue mutated in P1 and P2 was analyzed in the description of the structure of the IL-21R–IL-21 complex (Hamming et al., 2012), that analysis led us to focus on methods that would analyze the stability of the protein. We used MolProbity version 3.19 (Chen et al., 2010) and PoPMuSiC version 2.1 (Dehouck et al., 2011). To visualize the protein structure and set up the mutant structure, we used Swiss-PdbViewer version 4.01 (Guex et al., 1999) to model the Arg201Leu substitution, accepting the most favorable rotamer.

**RNA isolation, reverse transcription and quantification of gene expression.** RNA was isolated from stimulated B cells of P2 (day 6), Jurkat cells and HeLa cells (untransduced and transduced) before and after treatment with 50 ng/ml IL-21 using RNeasy Mini kit (QIAGEN) according to the manufacturer's protocol. Further, cDNA was synthesized with Expand Reverse transcription kit (Roche). Real-time PCR was performed on Applied Biosystems system (7900HT Fast Real-Time PCR; Applied Biosystems) using Power SYBR Green qPCR Master Mix (Applied Biosystems). Expression of *AICDA*, *PRDM1*, and *IL21R* was normalized to *RPS9* mRNA. The following primers were used: *AICDA*, forward 5′-GACTTTGGTTATCTTCGCAATAAGA-3′ and reverse 5′-AGGTCCCAGTCCGAGATGTA-3′; *PRDM1*, forward 5′-AACGTGTGGGTACGACCTTG-3′ and reverse 5′-ATTTTCATGGTCCCCTTGGT-3′; *RPS9*, forward 5′-AGACCCAGGTCTTCAAGCTG-3′ and reverse 5′-ATGAAGGACGGGATGTTCAC-3′.

Cycling conditions consisted of an initial activation of 15 min at 95°C, 35 cycles of denaturation at 95°C for 30 s, annealing at 55°C for 30 s, and elongation at 72°C for 30 s, followed by melting curve analysis to identify amplification of the correct PCR product.

**Microarray analysis.** PBMCs isolated from healthy donors and P2 from family A were stimulated with 1 µg/ml anti-CD3 (OKT-3) and 0.5 µg/ml anti-CD28 (3D10) for 0, 6, 12, and 18 h. Cells were collected and total RNA was isolated using an Absolutely RNA Purification kit (Stratagene) according to the manufacturer's instructions. cDNA preparation and DNA microarray analysis were performed at the Genomics Core Laboratory of the University Medical Center Freiburg, Germany. The image analysis was performed using AGCC software. Additional processing and analysis were completed with packages from the Bioconductor suite (Gentleman et al., 2004). The intensities were background corrected, normalized, and the expression values computed by Robust Microchip Average methodology. Subsequently, average fold changes between 0 and 6, 12, or 18 h of stimulation were calculated. Genes whose absolute log2 fold changes exceeded 1.0 in at least one of the comparisons were considered as potentially regulated upon stimulation. To analyze the expression profile of cytokines, we considered only genes annotated with at least one of the following gene ontology (GO) terms: GO:0008009 and GO:0005125. Data described in the paper have been deposited in National Center for Biotechnology Information's Gene Expression Omnibus under accession no. GSE29624.

**DNA constructs and lentiviral transduction.** For studying the role of IL-21R deficiency in case of family A, cDNA encoding for wild-type (wt, HsCD00076326, PlasmidID) or mutant (mut, Arg201Leu) human IL-21R was cloned into a bicistronic lentiviral pRRL vector coexpressing our gene of interest (*IL21R*) and an *enhanced GFP* (*eGFP*) marker gene via an EMCV IRES sequence. In addition, $\gamma_c$ cDNA was cloned into the same lentiviral backbone, but containing *dTomato* as a marker gene. For cell biology studies on IL-21R subcellular trafficking and IL-21 ligand binding, C-terminal fusion constructs of wild-type and mutant IL-21R were cloned on the basis of the generated bicistronic lentiviral pRRL vectors. VSVg-pseudotyped lentiviral particles were generated by transfection into 293T cells. In brief, $5 \times 10^6$ 293T cells were plated 24 h before virus transfection in 10-cm dishes. Using the calcium phosphate transfection method, we incubated cells with 5 µg lentiviral vector, 12 µg pcDNA3.GP.4xCTE (expressing HIV-1 gag/pol), 5 µg pRSV-Rev, and 1.5 µg pMD.G (which codes for VSV-g) in the presence of 25 µmol/liter chloroquine for 12 h. Supernatants containing viral particles were collected every 24 h for 72 h and concentrated by ultracentrifugation. Viral titration was performed on HT-1080 cells and determined by flow cytometry.

HeLa cells were first transduced with lentiviral particles encoding for $\gamma_c$ in the presence of 8 µg/ml polybrene for 12 h, followed by transduction of IL-21Rwt or IL-21Rmut. Transduction efficiency was determined by eGFP and dTomato expression using FACS.

**High-resolution APD imaging of mutated (Arg201Leu) IL-21R.** To analyze subcellular distribution of mutated IL-21R$^{Arg201Leu}$, we used HeLa cell lines stably coexpressing nonfluorescent $\gamma_c$ along with the C-terminally eGFP-tagged IL-21R (wild-type or mutant) and as a control HeLa cells expressing nonfluorescent $\gamma_c$ only. For imaging, we seeded 8-well, #1.5 Labtek slides (Thermo Fisher Scientific) at densities leading to stably adhered cells with ∼30–40% confluency after 24 h. For transfection with Takara Bio, Inc. pEGFP-N1–based mammalian expression vectors (pJAK3-TagRFP [RFP] and/or pIL-2Rg; Weidemann et al., 2011), 100–300 ng of plasmid were mixed with 30 µl of TurboFect solution (Thermo Fisher Scientific), incubated for 20 min and applied to each well. Live cell imaging was done in air buffer (150 mM NaCl, 20 mM Hepes pH 7.4, 15 mM Glucose, 46 mM trehalose, 5.4 mM KCl, 0.85 mM $MgSO_4$, 1.7 mM $CaCl_2$, and 0.15 mg/ml bovine serum albumin) at 22°C. Nuclei were stained by incubating the cells with DRAQ5 (1: 1000; BioStatus Limited) for 5 min at room temperature.

For confocal imaging, we used a LSM510/Confocor3 (Carl Zeiss) equipped with APD single-photon counting detectors. Sequential imaging was used to minimize spectral crosstalk between eGFP, TagRFP, and Atto647N.

**Fluorescence labeling of rh IL-21.** 100 µg rh IL-21 (molecular mass, 15.4 kD) was reconstituted in 200 µl $H_2O$ for 2 d at 8°C. From this, 5 nmol were supplemented with 2× labeling buffer (20 mM $NaHCO_3$ in 2× PBS). 1 mg of the aminoreactive dye Atto647N (ATTO-TEC; Siegen) was resuspended in 80 µl anhydrous DMSO from which 1 µl (threefold molar excess) was slowly added to the protein solution under constant agitation with a vortex machine. The coupling reaction was allowed for 2 h, followed by purification using Nap5 gel filtration columns (GE Healthcare). The protein was eluted drop-wise with labeling buffer. The fraction containing labeled protein showed OD (650 nm) = 0.043, which translates ($\varepsilon$ = 150,000 $M^{-1}cm^{-1}$) into 2.8 µM conjugated dye.

**Flow cytometry.** For immunophenotypical analysis, PBMCs were isolated by Ficoll density gradient and stained with monoclonal antibodies to characterize different lymphocyte subpopulations. The following antibodies were used (all from BD, unless noted otherwise): anti–CD1-FITC, anti–CD2-PE, anti–CD3-PeCy7, anti–CD4-PerCp, anti–CD8-Alexa Fluor 780 (eBioscience), anti–CD11a-PeCy5, anti–CD16-PE, anti–CD19-PeCy7, anti–CD20-PE, anti–CD25-PE, anti–CD27-Biotin, anti–CD40L-FITC, anti–CD56-PE, anti–IgD-FITC, anti–IgG-Biotin, anti–IgM-eFluor450/-APC (eBioscience), anti-HLA-DR-PeCy5, anti-TCR1-APC (eBioscience), anti–TCR2-PE, anti–MHC1-FITC, and anti–MHCII-V450. Analysis of IL-21R surface expression was performed using an anti–CD360-APC (BioLegend) antibody. Cells stained with biotinylated monoclonal antibodies were incubated with streptavidin-PerCP or -eFluor450 (eBioscience). Fluorescence intensity plots are shown in log scales.

To analyze the binding of fluorescently labeled rh IL-21-Atto647N to mutated IL-21R$^{Arg201Leu}$, HeLa cells expressing wild-type or mutant IL-21R-eGFP were harvested with cell dissociation buffer (Invtrogen), transferred into ice-cold PBS, and 5 × $10^5$ cells were distributed into 1.5-ml plastic vials. For staining, cells were pelleted and resuspended in 100 µl PBS containing 28 nM Atto647N conjugated to rh IL-21, incubated for 15 min on ice, and washed once with ice-cold PBS. Cells were then fixed with 3% paraformaldehyde (PFA) solution under constant agitation for 20 min at 4°C, followed by 5 min at room temperature, transferred into 13-ml FACS tubes (BD), and measured with a LSRII Flow Cytometer (BD). For excitation, we used the 488 and 633 nm laser lines, and for detection we used the 530/30-nm filter for eGFP and the 620/20-nm filter for Atto647N.

Analysis of IL-21R–mediated signal transduction in P3 and P4 of family B was performed using flow cytometry. PBMCs of healthy donors and patients were isolated from whole blood by Ficoll-Hypaque gradient centrifugation. To assay STAT1, STAT3, and STAT5 activation, PBMCs were serum starved for 30 min and stimulated either with rh IFN-γ (2,000 IU/ml), rh IL-6 (100 ng/ml), rh IL-21 (100 ng/ml), or rh IL-2 (40 IU/ml) for 15 min after fixation with paraformaldehyde and permeabilization in methanol. All recombinant cytokines were purchased from PeproTech. Cells were stained with Alexa Fluor 488–conjugated anti–phospho STAT1 (Tyr701), PE conjugated anti–phospho STAT3 (Tyr705), and Pacific Blue–conjugated anti-phospho STAT5 (Tyr694; all from BD). Levels of STAT phosphorylation were assessed in the $CD3^+$ lymphocyte gate.

**Western blot.** EBV-transformed B cells of P2 from family A, IL-21Rwt-$\gamma_c$– and IL-21Rmut-$\gamma_c$–transduced HeLa cells were starved for 12 h in serum-free medium before stimulation with rh IL-21 (50 ng/ml), IL-10 (50 ng/ml), IL-2 (100 ng/ml), IL-4 (100 ng/ml), IL-7 (100 ng/ml), or IL-15 (10 ng/ml). All cytokines were purchased from PeproTech, Hamburg, Germany. The stimulation was terminated by washing the cells with ice-cold PBS containing 1 mM sodium orthovanadate, followed by cell lysis. Western blot analyses were performed according to standard protocols. The following primary antibodies were used (all from BD, unless noted otherwise): anti–IL-21R (R&D Systems, Germany), anti–phospho-STAT1 (Tyr701), anti-STAT1, anti–phospho-STAT3 (Tyr705; Cell Signaling Technology), anti–phospho-STAT3 (Ser727; Cell Signaling Technology), anti-STAT3, anti-phospho-STAT5 (Tyr694), anti-STAT5, anti-phospho-STAT6 (Tyr641), anti-STAT6, anti-actin (Santa Cruz Biotechnology, Inc.), and anti-GAPDH (Santa Cruz Biotechnology). HRP-conjugated anti-mouse and anti-rabbit (Cell Signaling Technology) secondary antibodies were detected using a chemiluminescent substrate (Thermo Fisher Scientific). Images were captured on a Chemidoc XRS Imaging System (Bio-Rad Laboratories).

**Protein array.** PBMCs from healthy donors and P2 from family A were stimulated with 1 µg/ml anti-CD3 (OKT-3) and 0.5 µg/ml anti-CD28 (3D10) for 0, 6, 12, and 18 h. Supernatants were collected and subjected to quantitative analysis of secreted proteins using a Quantibody Human Th17 Array (RayBiotech) according to the manufacturer's protocol. Fluorescence signals were visualized using a laser scanner equipped with a Cy3 wavelength (DNA Microarray Scanner; Agilent Technologies) and data analysis was performed with ImaGene software using standard settings. Spots that failed the quality tests conducted by the software were excluded from further analysis. The preprocessing and the analysis of the intensity data were performed with the "limma" package (Smyth 2004) from the Bioconductor suite (Gentleman et al., 2004). The intensities of the spots were background corrected using "normexp" method and normalized using control spots. The intensities of spots belonging to a single cytokine antibody array were corrected (multiplied) by a factor. These factors were computed from two separate groups of control spots present on the array to decrease as much as possible the spread of the intensities across the whole array within each of the control groups. By fitting an appropriate linear model (assuming pairing of samples), fold changes were computed between 0 and 18 h. P-values and confidence intervals were computed by using the Bayes shrinkage method.

**B cell proliferation and differentiation assay.** Naive B cells ($CD19^+$ $IgD^{high}IgG^{low}CD27^{low}$) were sorted from PBMCs of healthy donors and P2 from family A. Further, cells were labeled with CFSE (1 µM; Molecular Probes) and cultured with 500 ng/ml Immunobead rabbit anti–human IgM-coated beads (Irvine Scientific) for 2 h (BCR engagement). Next, B cells (5 × $10^4$ cells/well of flat-bottom 96-well plate) were plated on the layer of 3T3-CD40L–expressing cells (to mimic cognate interactions with $CD4^+$ T cells), which were irradiated (70 Gy) 12 h before assay (2 × $10^4$ cells/well). For optimal stimulation, co-cultures were maintained in RPMI supplemented with 10% FCS, 20 U/ml rh IL-2 (cognate interactions with $CD4^+$ T cells; PeproTech) and 50 nM CpG (TLR9 engagement by microbial DNA; ODN2006; InvivoGen) for 6 d. B cell proliferation was determined by CFSE dilution, and immunoglobulin class-switch was measured by surface expression of IgG and IgA using flow cytometry. Cells were stimulated with 10 ng/ml IL-21 (PeproTech) alone or with 1 ng/ml TGF-β (PeproTech). CD40L/IL-21–induced B cell proliferation and immunoglobulin class-switch in P3 and P4 were performed as previously described (Recher et al., 2011).

**T cell proliferation assay.** To analyze T cell proliferation, $10^5$ PBMCs were cultured in RPMI 1640 medium supplemented with 10% FCS, 100 U/ml penicillin/streptomycin, 10 mM Hepes, 10 mM nonessential amino acids, 10 mM sodium pyruvate, and 50 µM 2-mercaptoethanol in the presence of the following stimuli: immobilized 1 µg/ml anti-CD3 (OKT-3; BD), 10 ng/ml IL-2 (PeproTech), 10 ng/ml phytohemagglutinin (PHA; Sigma-Aldrich), 5 µg/ml ConA (Sigma-Aldrich), and 0.5 µg/ml pokeweed mitogen (PWM; Sigma-Aldrich). T cell stimulation with DTT and TT (The Binding Site GmbH; 0.5 Limes fl occulation [Lf]/ml) was performed on flat-bottom 96-well plates ($10^5$ PBMCs/well) in complete RPMI 1640 supplemented with 5% human serum.

In each experiment, T cells were cultured for 48 h, pulsed with 1 µCi (0.037 MBq) [$^3$H]-thymidine (GE Healthcare) for an additional 16 h, harvested, and analyzed for thymidine incorporation (cpm).

Lymphocyte function (T cell proliferation and mixed lymphocyte reaction) in P3 and P4 was evaluated as previously outlined in principle (Garcia-Piñeres et al., 2006).

**NK cell assay.** Standard $^{51}$Chromium ($^{51}$Cr) release cytotoxicity assays were performed using K562 and L1210 cell lines (German Collection of Microorganisms and Cell Cultures, DMSZ, Braunschweig, Germany) as targets (Jacobs et al., 2001). K562 and L1210 cells ($2 \times 10^6$) were labeled with 3 MBq $Na_2{}^{51}CrO_4$ (Hartmann) for 1 h and washed three times. L1210 cells were incubated for 30 min with rabbit anti-L1210 serum (Department of Clinical Immunology and Rheumatology, Medical School Hannover, Hannover, Germany). After three washes, target cells ($5 \times 10^3$/50 µl) were seeded in 96-well V-bottom plates. Effector cells (freshly isolated PBMCs) were added in defined effector/target (E/T) cell ratios (60:1, 30:1, 15:1, and 7.5:1). For determination of spontaneous and maximum $^{51}$Cr release, cells were cultured in media alone or lysed in 1% Triton X-100 (Sigma-Aldrich). Specific cytotoxicity was detected by measuring the release of $^{51}$Cr using a Microbeta 1450 counter (Perkin Elmer) after 4 h of incubation. Specific lysis was calculated using following formula: ([experimental release − spontaneous release]/[release maximum − spontaneous release]) × 100. NK cell function in P3 and P4 of family B was analyzed by the Diagnostic Immunology Laboratory at Cincinnati Children's Hospital and provided as a commercially available diagnostic service.

**Online supplemental material.** Fig. S1 shows the clinical and histopathological phenotype of P1 and P2 from family A. Table S1 lists variant calling statistics for NGES of kindred A. Table S2 shows gene expression profile of Th1-, Th2-, and Th17-associated cytokines in IL-21R–deficient P2. Table S3 lists primers for Sanger sequencing of *IL21R* and *RAB3IL1*. Online supplemental material is available at http://www.jem.org/cgi/content/full/jem.20111229/DC1.

We thank the interdisciplinary medical team and clinicians involved in the care of these patients. We thank Dr. Rachel Brown (University Hospital Birmingham, Birmingham, UK) for performing immunohistochemistry studies on P1, Drs. Hamming and Hartmann (Aarhus University, Aarhus, Denmark) for providing the structure file of IL-21R bound to IL-21 before it was available via the Protein Data Bank, Mr. Brian H. Santich for sorting of naive B cells at National Institute of Allergy and Infectious Diseases, and Dr. Shannon Glaser (Scott & White Disease Research Center, Temple, Texas) for providing us with cholangiocyte and cholangiocarcinoma cell lines. We dedicate this work to the deceased P1 and P2 and their family.

The study is supported by grants from DFG (KFO250, SFB900, Gottfried-Wilhelm-Leibniz Program), BMBF (PID-NET), E-RARE, DAAD, REBIRTH (EXC62/1), Care-for-Rare Foundation, and Deutsche José Carreras Leukämie-Stiftung (fellowship to D. Kotlarz). This research is supported in part by the Intramural Research Program of the NIH, NIAID, NIAMS, and NLM.

The authors declare no competing financial interests.

**Submitted: 16 June 2011**
**Accepted: 9 January 2013**

## REFERENCES

Altschul, S.F., T.L. Madden, A.A. Schäffer, J. Zhang, Z. Zhang, W. Miller, and D.J. Lipman. 1997. Gapped BLAST and PSI-BLAST: a new generation of protein database search programs. *Nucleic Acids Res.* 25:3389–3402. http://dx.doi.org/10.1093/nar/25.17.3389

Casanova, J.-L., and L. Abel. 2007. Primary immunodeficiencies: a field in its infancy. *Science*. 317:617–619. http://dx.doi.org/10.1126/science.1142963

Chen, V.B., W.B. Arendall III, J.J. Headd, D.A. Keedy, R.M. Immormino, G.J. Kapral, L.W. Murray, J.S. Richardson, and D.C. Richardson. 2010. MolProbity: all-atom structure validation for macromolecular crystallography. *Acta Crystallogr. D Biol. Crystallogr.* 66:12–21. http://dx.doi.org/10.1107/S0907444909042073

Dehouck, Y., J.M. Kwasigroch, D. Gilis, and M. Rooman. 2011. PoPMuSiC 2.1: a web server for the estimation of protein stability changes upon mutation and sequence optimality. *BMC Bioinformatics*. 12:151. http://dx.doi.org/10.1186/1471-2105-12-151

Ettinger, R., G.P. Sims, A.-M. Fairhurst, R. Robbins, Y.S. da Silva, R. Spolski, W.J. Leonard, and P.E. Lipsky. 2005. IL-21 induces differentiation of human naive and memory B cells into antibody-secreting plasma cells. *J. Immunol.* 175:7867–7879.

Fröhlich, A., J. Kisielow, I. Schmitz, S. Freigang, A.T. Shamshiev, J. Weber, B.J. Marsland, A. Oxenius, and M. Kopf. 2009. IL-21R on T cells is critical for sustained functionality and control of chronic viral infection. *Science*. 324:1576–1580. http://dx.doi.org/10.1126/science.1172815

García-Piñeres, A.J., A. Hildesheim, M. Williams, M. Trivett, S. Strobl, and L.A. Pinto. 2006. DNAse treatment following thawing of cryopreserved PBMC is a procedure suitable for lymphocyte functional studies. *J. Immunol. Methods*. 313:209–213. http://dx.doi.org/10.1016/j.jim.2006.04.004

Gentleman, R.C., V.J. Carey, D.M. Bates, B. Bolstad, M. Dettling, S. Dudoit, B. Ellis, L. Gautier, Y. Ge, J. Gentry, et al. 2004. Bioconductor: open software development for computational biology and bioinformatics. *Genome Biol.* 5:R80. http://dx.doi.org/10.1186/gb-2004-5-10-r80

Glocker, E.-O., D. Kotlarz, K. Boztug, E.M. Gertz, A.A. Schäffer, F. Noyan, M. Perro, J. Diestelhorst, A. Allroth, D. Murugan, et al. 2009. Inflammatory bowel disease and mutations affecting the interleukin-10 receptor. *N. Engl. J. Med.* 361:2033–2045. http://dx.doi.org/10.1056/NEJMoa0907206

Guex, N., A. Diemand, and M.C. Peitsch. 1999. Protein modelling for all. *Trends Biochem. Sci.* 24:364–367. http://dx.doi.org/10.1016/S0968-0004(99)01427-9

Hamming, O.J., L. Kang, A. Svensson, J.L. Karlsen, H. Rahbek-Nielsen, S.R. Paludan, S.A. Hjorth, K. Bondensgaard, and R. Hartmann. 2012. Crystal structure of interleukin-21 receptor (IL-21R) bound to IL-21 reveals that sugar chain interacting with WSXWS motif is integral part of IL-21R. *J. Biol. Chem.* 287:9454–9460. http://dx.doi.org/10.1074/jbc.M111.311084

Hilton, D.J., S.S. Watowich, L. Katz, and H.F. Lodish. 1996. Saturation mutagenesis of the WSXWS motif of the erythropoietin receptor. *J. Biol. Chem.* 271:4699–4708. http://dx.doi.org/10.1074/jbc.271.23.13754

Jacobs, R., C.R. Pawlak, E. Mikeska, D. Meyer-Olson, M. Martin, C.J. Heijnen, M. Schedlowski, and R.E. Schmidt. 2001. Systemic lupus erythematosus and rheumatoid arthritis patients differ from healthy controls in their cytokine pattern after stress exposure. *Rheumatology (Oxford).* 40:868–875. http://dx.doi.org/10.1093/rheumatology/40.8.868

Kasaian, M.T., M.J. Whitters, L.L. Carter, L.D. Lowe, J.M. Jussif, B. Deng, K.A. Johnson, J.S. Witek, M. Senices, R.F. Konz, et al. 2002. IL-21 limits NK cell responses and promotes antigen-specific T cell activation: a mediator of the transition from innate to adaptive immunity. *Immunity*. 16:559–569. http://dx.doi.org/10.1016/S1074-7613(02)00295-9

Klein, C., B. Lisowska-Grospierre, F. LeDeist, A. Fischer, and C. Griscelli. 1993. Major histocompatibility complex class II deficiency: clinical manifestations, immunologic features, and outcome. *J. Pediatr.* 123:921–928. http://dx.doi.org/10.1016/S0022-3476(05)80388-9

Krawitz, P., C. Rödelsperger, M. Jäger, L. Jostins, S. Bauer, and P.N. Robinson. 2010. Microindel detection in short-read sequence data. *Bioinformatics*. 26:722–729. http://dx.doi.org/10.1093/bioinformatics/btq027

Ku, C.S., N. Naidoo, and Y. Pawitan. 2011. Revisiting Mendelian disorders through exome sequencing. *Hum. Genet.* 129:351–370. http://dx.doi.org/10.1007/s00439-011-0964-2

Li, H., B. Handsaker, A. Wysoker, T. Fennell, J. Ruan, N. Homer, G. Marth, G. Abecasis, and R. Durbin; 1000 Genome Project Data Processing Subgroup. 2009. The Sequence Alignment/Map format and SAMtools. *Bioinformatics*. 25:2078–2079. http://dx.doi.org/10.1093/bioinformatics/btp352

Ng, P.C., and S. Henikoff. 2002. Accounting for human polymorphisms predicted to affect protein function. *Genome Res.* 12:436–446. http://dx.doi.org/10.1101/gr.212802

Nurieva, R., X.O. Yang, G. Martinez, Y. Zhang, A.D. Panopoulos, L. Ma, K. Schluns, Q. Tian, S.S. Watowich, A.M. Jetten, and C. Dong. 2007. Essential autocrine regulation by IL-21 in the generation of inflammatory T cells. *Nature*. 448:480–483. http://dx.doi.org/10.1038/nature05969

Ozaki, K., K. Kikly, D. Michalovich, P.R. Young, and W.J. Leonard. 2000. Cloning of a type I cytokine receptor most related to the IL-2 receptor β chain. *Proc. Natl. Acad. Sci. USA*. 97:11439–11444. http://dx.doi.org/10.1073/pnas.200360997

Ozaki, K., R. Spolski, C.G. Feng, C.-F. Qi, J. Cheng, A. Sher, H.C. Morse III, C. Liu, P.L. Schwartzberg, and W.J. Leonard. 2002. A critical role for IL-21 in regulating immunoglobulin production. *Science*. 298:1630–1634. http://dx.doi.org/10.1126/science.1077002

Parrish-Novak, J., D.C. Foster, R.D. Holly, and C.H. Clegg. 2002. Interleukin-21 and the IL-21 receptor: novel effectors of NK and T cell responses. *J. Leukoc. Biol.* 72:856–863.

Pesce, J., M. Kaviratne, T.R. Ramalingam, R.W. Thompson, J.F. Urban Jr., A.W. Cheever, D.A. Young, M. Collins, M.J. Grusby, and T.A. Wynn. 2006. The IL-21 receptor augments Th2 effector function and alternative macrophage activation. *J. Clin. Invest.* 116:2044–2055. http://dx.doi.org/10.1172/JCI27727

Quinlan, A.R., and I.M. Hall. 2010. BEDTools: a flexible suite of utilities for comparing genomic features. *Bioinformatics*. 26:841–842. http://dx.doi.org/10.1093/bioinformatics/btq033

Ramensky, V., P. Bork, and S. Sunyaev. 2002. Human non-synonymous SNPs: server and survey. *Nucleic Acids Res.* 30:3894–3900. http://dx.doi.org/10.1093/nar/gkf493

Rankin, A.L., H. MacLeod, S. Keegan, T. Andreyeva, L. Lowe, L. Bloom, M. Collins, C. Nickerson-Nutter, D. Young, and H. Guay. 2011. IL-21 receptor is critical for the development of memory B cell responses. *J. Immunol.* 186:667–674. http://dx.doi.org/10.4049/jimmunol.0903207

Recher, M., L.J. Berglund, D.T. Avery, M.J. Cowan, A.R. Gennery, J. Smart, J. Peake, M. Wong, S.-Y. Pai, S. Baxi, et al. 2011. IL-21 is the primary common γ chain-binding cytokine required for human B-cell differentiation in vivo. *Blood*. 118:6824–6835. http://dx.doi.org/10.1182/blood-2011-06-362533

Salzer, U., C. Bacchelli, S. Buckridge, Q. Pan-Hammarström, S. Jennings, V. Lougaris, A. Bergbreiter, T. Hagena, J. Birmelin, A. Plebani, et al. 2009. Relevance of biallelic versus monoallelic *TNFRSF13B* mutations in distinguishing disease-causing from risk-increasing *TNFRSF13B* variants in antibody deficiency syndromes. *Blood*. 113:1967–1976. http://dx.doi.org/10.1182/blood-2008-02-141937

Smyth, G.K. 2004. Linear models and empirical bayes methods for assessing differential expression in microarray experiments. *Stat. Appl. Genet. Mol. Biol.* 3:e3. http://dx.doi.org/10.2202/1544-6115.1027

Spolski, R., and W.J. Leonard. 2008. Interleukin-21: basic biology and implications for cancer and autoimmunity. *Annu. Rev. Immunol.* 26:57–79. http://dx.doi.org/10.1146/annurev.immunol.26.021607.090316

Thusberg, J., and M. Vihinen. 2006. Bioinformatic analysis of protein structure-function relationships: case study of leukocyte elastase (ELA2) missense mutations. *Hum. Mutat.* 27:1230–1243. http://dx.doi.org/10.1002/humu.20407

Weidemann, T., R. Worch, K. Kurgonaite, M. Hintersteiner, C. Bökel, and P. Schwille. 2011. Single cell analysis of ligand binding and complex formation of interleukin-4 receptor subunits. *Biophys. J.* 101:2360–2369. http://dx.doi.org/10.1016/j.bpj.2011.10.014

Wolska-Kusnierz, B., A. Bajer, S. Caccio, E. Heropolitanska-Pliszka, E. Bernatowska, P. Socha, J. van Dongen, M. Bednarska, A. Paziewska, and E. Sinski. 2007. *Cryptosporidium* infection in patients with primary immunodeficiencies. *J. Pediatr. Gastroenterol. Nutr.* 45:458–464. http://dx.doi.org/10.1097/MPG.0b013e318054b09b

Zhou, L., I.I. Ivanov, R. Spolski, R. Min, K. Shenderov, T. Egawa, D.E. Levy, W.J. Leonard, and D.R. Littman. 2007. IL-6 programs $T_{(H)}$-17 cell differentiation by promoting sequential engagement of the IL-21 and IL-23 pathways. *Nat. Immunol.* 8:967–974. http://dx.doi.org/10.1038/ni1488